Clinical and Translational Radiation Oncology 49 (2024) 100863

Contents lists available at ScienceDirect

Clinical and Translational Radiation Oncology

journal homepage: www.sciencedirect.com/journal/clinical-and-translational-radiation-oncology

Original Research Article

Immunological responses to brain metastasis stereotactic radiosurgery in patient-matched longitudinal blood and tumour samples

Joseph Sia [a,b,*], Criselle D'Souza [b,c], Becky Castle [b,c], Yu-Kuan Huang [b,c], Han Xiang Aw Yeang [b,d], Rejhan Idrizi [d], Metta Jana [d], Shankar Siva [a,b], Claire Phillips [a,b,1], Paul Neeson [b,c,1]

[a] Department of Radiation Oncology, Peter MacCallum Cancer Centre, Melbourne 3000, Australia
[b] Sir Peter MacCallum Department of Oncology, University of Melbourne, Melbourne 3010, Australia
[c] Cancer Immunology Program, Peter MacCallum Cancer Centre, Melbourne 3000, Australia
[d] Centre for Advanced Histology and Microscopy, Peter MacCallum Cancer Centre, Melbourne 3000, Australia

ARTICLE INFO

Keywords:
Brain metastases
Stereotactic radiation therapy
Radiotherapy
Tumour immunology

ABSTRACT

Background: Stereotactic radiosurgery (SRS) is highly effective as focal treatment for brain metastases (BrMs), but whether it can promote anti-tumour immune responses that synergise with immunotherapy remains unclear. We investigated this by examining blood samples from a clinical trial for HER2-amplified breast cancer (HER2-BC) BrMs, matched with longitudinal HER2-BC BrM samples resected from the same location in the same patient.
Methods: Blood samples from 10 patients taken pre- and 7–14 days post-SRS were analysed by mass and flow cytometry. One patient received pre-operative SRS for a BrM that recurred 7 months after resection, followed by planned re-resection 8 days post-SRS. Pre- and post-SRS tumours from this patient were analysed by bulk RNAseq, multiplex immunohistochemistry (mIHC), and TCR sequencing.
Results: Monocytes, central memory CD8+ T and regulatory T cells were enriched in blood post-SRS, together with increased MHC-II expression on monocytes, conventional DCs, and monocytic MDSCs. In tumour, SRS upregulated antigen presentation, T cell proliferation and T cell co-stimulation signatures, alongside an influx of tumour-associated macrophages (TAMs) and CD4+ T cells. Specifically, TAMs and CD4+ T cells, but not CD8+ T cells, demonstrated spatial co-localisation post-SRS. These TAMs were lowly PD-L1 expressing, but CD4+ T cells showed increased PD-1 expression. A sizeable proportion of T cell clonotypes were retained post-SRS, and four clones demonstrated significant, non-stochastic expansion.
Conclusion: Systemic and local immunological changes in this homogenous patient cohort suggest that SRS may facilitate MHC-II-restricted T cell priming responses involving the monocyte-macrophage lineage and CD4+ T cells, which should be further explored.

1. Introduction

Brain metastases (BrMs) afflict about half of patients with advanced cancer, cause multi-domain impairment on quality of life, and are almost universally associated with a poor prognosis [1]. Paradoxically, as newer systemic therapies improve patient survival across cancer types, the late emergence of BrMs, which can be persistently recurrent and devastating despite well-controlled extracranial disease, is increasingly a problem in the clinic [2].

Although clinical trials have shown immune checkpoint blockade (ICB) can achieve durable BrM responses, these are restricted to asymptomatic melanoma and non-small cell lung cancer (NSCLC) BrMs requiring low-dose or no concurrent corticosteroid use [3–5]. There is clinical data to suggest broadened and improved intracranial activity of ICB when combined with stereotactic radiosurgery (SRS) [6–9] – a commonly used, highly precise form of radiation therapy (RT) that targets individual BrMs while sparing surrounding normal brain. Compellingly, this parallels growing clinical and translational data in the extracranial setting suggesting ICB and RT can exert synergistic, non-overlapping immunological effects against cancer [10,11].

* Corresponding author at: Department of Radiation Oncology, Peter MacCallum Cancer Centre, 305 Grattan Street, Melbourne, VIC 3000, Australia.
E-mail address: joseph.sia@petermac.org (J. Sia).
[1] Senior Authors.

https://doi.org/10.1016/j.ctro.2024.100863
Received 5 June 2024; Received in revised form 30 August 2024; Accepted 20 September 2024
Available online 21 September 2024

A lack of instructive data on the immunological impact of SRS in the brain, nonetheless, is a critical knowledge gap in optimising this strategy for BrMs. In addition to the challenge of accessing BrM tissue, SRS-treated BrMs are often resected only following tumour recurrence, thus unfairly representing the majority of cases in which SRS achieves excellent BrM control [12]. Furthermore, overcoming inter-tumour heterogeneity would require longitudinal sampling of the same BrM, which is rarely performed. These biases conceal bona fide SRS effects and likely underlie the conflicting observations in the limited number of reports thus far [13–16].

Here, we examined a cohort of peripheral blood samples taken before and after SRS in a clinical trial for HER2-amplified breast cancer BrMs, matched with a pair of pre- and post-SRS BrM samples of the same histology resected from the same location in the same patient, not complicated by treatment resistance. We observed changes suggesting SRS may be able to induce T cell priming involving macrophages and CD4+ T cells, which have therapeutic implications when considered alongside clinical reports of improved whole-brain metastatic control, beyond the SRS-treated site, when ICB is given concurrently with SRS [6–8], and the correlation of this phenomenon with increased circulating lymphocyte count [9].

2. Methods and materials

2.1. Human patients and biospecimen collection

Blood and BrM tumour tissue were collected from patients enrolled in the translational sub-study of the multi-centre Trans-Tasman Radiation Oncology Group (TROG) 16.02 Phase 2 clinical trial (ACTRN12616001265460) [17] (Supplementary Table 1). Patient informed consent was obtained and the trial, including the translational sub-study, was approved by the Peter MacCallum Cancer Centre Human Research Ethics Committee. Median follow-up duration was calculated using the inverse Kaplan-Meier method. Time to local failure and development of new BrMs were calculated using the Kaplan-Meier method. For the patient from whom pre- and post-SRS BrM tumours were obtained, a 20 Gy single fraction of neoadjuvant SRS was delivered 8 days prior to planned neurosurgical resection. The patient was on trastuzumab emtansine (T-DM1) at time of surgery and SRS. No concurrent ICB or dexamethasone was given. Blood and tumour tissue were collected and processed as described in Supplementary Methods.

2.3. Cytometry by time of flight (CyTOF) and cytokine analysis

CyTOF staining of blood samples was performed according to established protocols [18]. For details, refer Supplementary Methods. The antibody list is provided in Supplementary Table 2 and immune cell clusters were annotated as per Supplementary Table 3 and Supplementary Fig. 1. Plasma concentration level of cytokines were assessed as described in Supplementary Methods.

2.4. Gene expression analysis

RNA and DNA were extracted from tumour tissue for sequencing as described in Supplementary Methods. Gene signature scores were calculated using the single sample Gene Set Enrichment Analysis (ssGSEA) method with the GSVA package [19], with gene sets taken from the MSigDB C5 Ontology Gene Set (version 7.2). Transcriptome deconvolution to infer cell type abundances was performed with CIBERSORTx [20], using a breast cancer BrM-specific gene signature matrix created by combining the 3 breast cancer BrM single-cell RNA sequencing data from Gonzalez et al [21].

2.5. Diaminobenzidine (DAB) immunohistochemistry (IHC) and multiplex IHC (mIHC) staining

DAB and mIHC staining was performed as per described in Supplementary Methods. Tumour and normal brain regions were delineated by a neuro-oncology anatomical pathologist. Counting of cellular phenotypes was performed in HALO (Indigo Labs, USA) and corroborated with the SPIAT package [22]. Average minimum distances and cellular neighbourhood analyses were performed in SPIAT. For identification of cellular neighbourhoods, the minimum cluster size was set at 30 cells over a 70 μm radius.

2.6. T cell receptor (TCR) sequencing

Tumour genomic DNA was sent for deep TCRB sequencing with ImmunoSEQ (Adaptive Biotech, USA). Repertoire diversity, overlap and clonotype tracking were analysed with the immunarch package [23]. Differential abundance analysis was performed in the Adaptive ImmunoSEQ Analyser (Adaptive Biotech, USA). The CDR3 sequences of differentially abundant clonotypes were matched for any known antigen specificity in the VDJDb (updated 1 June 2023) [24] and McPAS-TCR (updated 10 September 2022) [25] databases.

3. Results

3.1. SRS for BrMs modulates an immune response detectable in peripheral blood

We examined 18 pre- and post-SRS blood samples (of which 16 were patient-paired) from 10 patients enrolled on the translational sub-study of a Phase 2 clinical trial, conducted to examine patterns of intracranial failure following local BrM therapy (neurosurgery and/or SRS) without whole-brain RT in patients with HER2-amplified breast cancer (Fig. 1a) [17]. 12 intact BrMs and 3 BrM cavities were treated with SRS in this sub-study with minimal concurrent corticosteroid use (Supplementary Table 1). With a median follow-up duration of 50.3 months, two local failures were observed at 13 and 16 months, and the median time to development of new BrMs (distant brain failure) was 27.5 months (Fig. 1b).

First-order clustering of lymphocyte and myeloid populations in blood using cytometry by time-of-flight (CyTOF) revealed a prominent trend for an increase in myeloid cells following SRS, while the other major cell types were largely unchanged (Supplementary Fig. 2). Sub-clustering revealed this myeloid enrichment to be driven by classical and intermediate monocytes, alongside a drop in conventional dendritic cells (cDCs) (Fig. 1c). Of the αβ T cells, we observed an SRS-induced increase in regulatory T (T_{reg}) and central memory CD8+ T (CD8+ T_{CM}) cells, while naïve CD4+ T (CD4+ T_{naive}) and CD4+ T_{EMRA} cells were diminished (Fig. 1c).

Interestingly, these changes were accompanied by increased expression of MHC-II (HLA-DR) on cDCs, as well as PD-L1 on classical monocytes, cDCs, and monocytic myeloid-derived suppressor cells (mMDSCs) (Fig. 1d). These immune cell types share a monocytic link, in that monocytes can differentiate into DCs closely resembling MHC-II-high Type 2 cDCs [26], and mMDSCs are aberrant precursors of monocytes under inflammatory myelopoietic signalling [27]. Modulation of T cell states following SRS was much more subdued (Supplementary Fig. 3).

Given these findings, we asked if alterations in inflammatory cytokines and myeloid growth factors could be detected in peripheral blood. In a panel of 20 cytokines tested, concentration of stem cell factor (SCF), a multi-function haematopoietic factor that can synergise with granulocyte–macrophage colony-stimulating factor (GM-CSF) for monocyte lineage commitment [28], showed a significant increase post-SRS (Supplementary Fig. 4). No significant changes in other cytokines, including MCP-1 (CCL2), IFN-γ, and IFN-α were detectable.

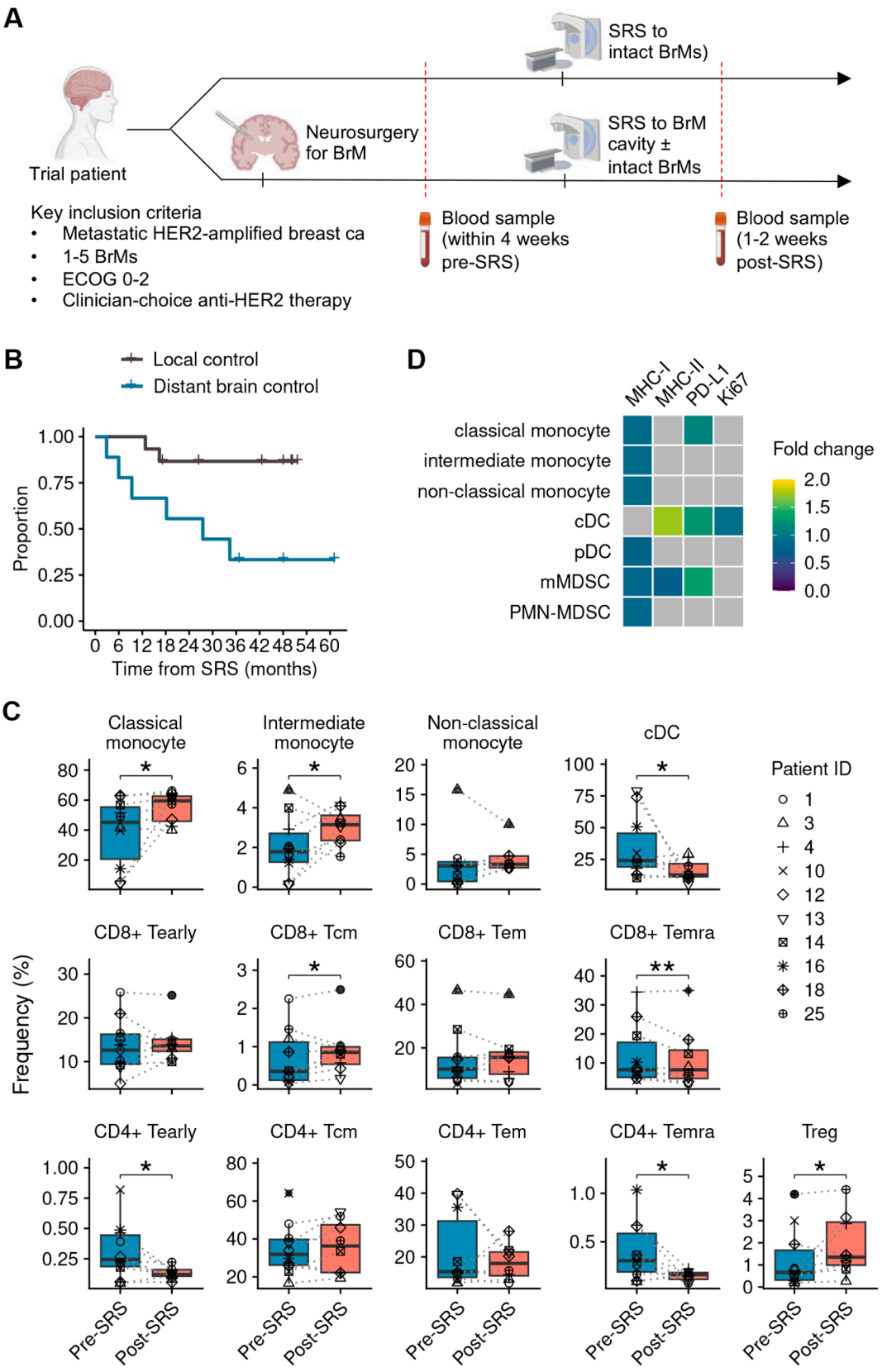

Fig. 1. SRS to BrMs modulates an immune response detectable in peripheral blood A. Schema of trial and blood collection time points **B.** Time to local failure and distant brain failure (development of new BrMs) in the patient cohort **C.** Immune cell subset frequencies in peripheral blood pre- and post-SRS (by CyTOF). * $p < 0.05$, adjusted $p \leq 0.1$ (generalised linear mixed model accounting for patient pairing) **D.** Changes in intensity of immune cell surface marker expression following SRS (by CyTOF). Grey squares represent non-significant modulation (adjusted $p > 0.1$, generalised linear mixed model accounting for patient pairing).

Collectively, these findings suggest that SRS for BrMs resulted in a systemic response involving monocytes and T cells.

3.2. Antigen presentation and T cell responses occur in the SRS-treated tumour

To investigate the origin of these peripheral responses, we interrogated a pair of BrMs pre- and post-SRS obtained from the same brain tumour location in the same patient (Fig. 2a, Methods). This patient presented with a solitary occipital BrM which was initially treated with SRS as part of this clinical trial, but recurred locally 2 years later, at which point SRS local control rates generally drop to 50–60 % [29]. This was resected (comprising the pre-SRS sample) with residual disease that progressed shortly within the BrM cavity. The cavity recurrence was then treated with neoadjuvant SRS followed by planned neurosurgical resection 8 days later (comprising the post-SRS sample). No translational blood samples were collected surrounding these events as they occurred after conclusion of the trial.

On gene expression profiling, immunological and neuronal transcriptional programs were most enriched following SRS, among which are T cell activation via antigen presentation, T cell proliferation and T cell co-stimulation (Fig. 2b, Supplementary Figure 5). Outside those represented by these gene signatures, well-described genes for T cell activation, inhibition, exhaustion, and cytotoxicity also showed an overall pattern of upregulation, including *TOX*, a regulator of tumour-specific T cell differentiation [30] (Fig. 2c).

To determine the composition of cell types that may contribute to these processes, we used a breast cancer BrM-specific signature matrix from published single-cell RNA sequencing data of BrMs [21] to deconvolute the bulk transcriptome. This inferred a significant loss of metastatic tumour cells in the post-SRS sample, as expected following SRS and thus serving as an internal control, and an expansion of the immune cell compartment (Fig. 2d). The immune cell increase was primarily accounted by *APOE*+/*C1QB*+ (APOE+) tumour-associated macrophages (TAMs) (19.6-fold), followed by CD4+ T_{CM} cells (2.6-fold) and *S100A8*+/*FCN1*+ (S100A8+) TAMs (2.0-fold). The proportion of CD8+ T cells was low and not significantly altered by SRS. Notably, APOE+ TAMs are described to express a core set of immunomodulatory molecules involved in antigen processing and presentation, while S100A8+ TAMs express an inflammatory program resembling MDSCs, neither of which fall neatly into classical M1/M2 phenotypes [21]. Using an independent gene signature for brain macrophage ontogeny [31], we confirmed that the post-SRS tumour strongly skewed towards being predominantly composed of bone marrow-derived macrophages (BMDMs) rather than brain-resident microglia (Fig. 2e).

The expansion of TAMs and the increase in peripheral monocytes at a similar timepoint following SRS (Fig. 1c) suggests an SRS-induced chemotactic process between the two tissue compartments. Inspection of chemokine transcript expression in the tumour revealed the top 3 upregulated members to be *CCL2*, *CCL3*, and *CXCL14*, all of which are major monocyte chemokines (Fig. 2f). However, there was no increased plasma concentration of MCP-1 (*CCL2*) detectable post-SRS in the peripheral blood cohort (Supplementary Fig. 4), and the transcript for SCF (*KITLG*) was not differentially expressed in this tumour pair ($|\text{fold change}| < 0.05$). Issues with detection of free/bound protein and inter-tumour heterogeneity may contribute to this apparent discordance.

3.3. Tumour-associated macrophages and CD4+ T cells cluster following SRS

Next, we sought to confirm the cell type abundances and explore their spatial distribution in tumour. The pre-SRS BrM demonstrated sequestration of immune cells in the perivascular niche outside tumour cell nests in an immune-excluded phenotype, although sparse CD8+ T cells were seen inside the tumour margin (Fig. 3a). This phenotype was abolished in the post-SRS specimen, showing significant loss of tumour cells, and immune cells interspersed among areas of necrosis, cellular debris, and small tumour cell islets (Fig. 3a). There were also more areas of normal brain parenchyma in the post-SRS specimen (Supplementary Figure 6), which was a surgical artefact that likely explains the neuronal signatures and astrocyte abundance inferred post-SRS (Supplementary Figure 5, Fig. 2d). Validating the deconvolution data, TAMs and specifically CD4+ T cells, but not CD8+ T cells, were highly enriched throughout tumour and brain regions (Fig. 3b).

Both pre- and post-SRS BrM TAMs were lowly PD-L1-expressing (Fig. 3c). However, PD-1 expression on CD4+ T cells unambiguously increased post-SRS, alongside elevated PD-1 and PD-L1 expression on CD8+ T and tumour cells respectively (Fig. 3c), together suggesting a non-inert immune infiltrate. Visually, there were areas in the post-SRS BrM, but not pre-SRS, where TAMs aggregated closely around tumour cells and CD4+ T cells (Fig. 3d). Indeed, minimum distances from the closest TAM (target cell type) to each tumour, CD4+ T, and CD8+ T cell (reference cell types) were significantly shorter post-SRS (Fig. 3e). Because this parameter is dependent on the target/reference cell order, the inverse was not uniformly true, whereby we saw shorter minimum distances from the closest tumour cell (target cell type) to each TAM, CD4+ and CD8+ T cell (reference cell types) pre-SRS, due to tumour nests bordering perivascular spaces in which immune cells segregated (Fig. 3a, e). Interestingly, activated CD4+ T cells, as determined by their PD-1 expression, were closely surrounded by TAMs, but activated CD8+ T cells did not demonstrate this proximity gradient (Fig. 3f).

Given these findings, we systematically searched for all cell clusters throughout the sample to discern what cell types tended to group together. By performing neighbourhood analysis using hierarchical clustering of cell–cell distances, 68 groups of closely spaced cells were identified among the primary pattern of free-standing cells in hypocellular regions (Fig. 3g). Very few clusters were comprised of a single cell type, but the majority were made up of either TAM-CD4+ T cell or TAM-tumour cell admixtures (Fig. 3h). In some clusters, three or four of the TAM, CD4+ T, CD8+ T, and tumour cell types could be found (Fig. 3d, h).

Thus, we observed changes of potential biological relevance in the immune and tumour cell spatial distribution following SRS, which propose the possibility of MHC-II-restricted interactions driving the transcriptional signatures of T cell receptor (TCR) contact and T cell activation observed earlier.

3.4. T cell clones are retained and differentially abundant in the SRS-treated tumour

We posited if antigen presentation was indeed occurring and leading to successful T cell priming, T cell clonal expansion would follow, resulting in an observable shift in tumour-associated TCR diversity. Uniquely, we were able to test this because the tumours were longitudinally obtained from the same tumour site pre- and post-SRS.

TCR sequencing of bulk tumour-derived DNA revealed a drop in repertoire richness and a rise in clonality following SRS (Fig. 4a). A moderate proportion of T cell clonotypes was retained with SRS, and the overlap of pre- and post-SRS repertoires (accounting for individual clonotypes and their abundance) was sizeable (Fig. 4b). The top clonotypes post-SRS were mostly shared with and expanded from those present pre-SRS except for one, which was *de novo* in tumour (Fig. 4c, d).

Importantly, four of these were statistically significant in their increased abundance, therefore unlikely explained by chance observation or by random replacement from circulating bystander T cells (Fig. 4d). One clonotype was significantly contracted. None of these differentially abundant clones matched any known TCR sequences against common viral and bacterial epitopes [24,25].

4. Discussion

In this study, we provide insight on how SRS for BrMs may shape

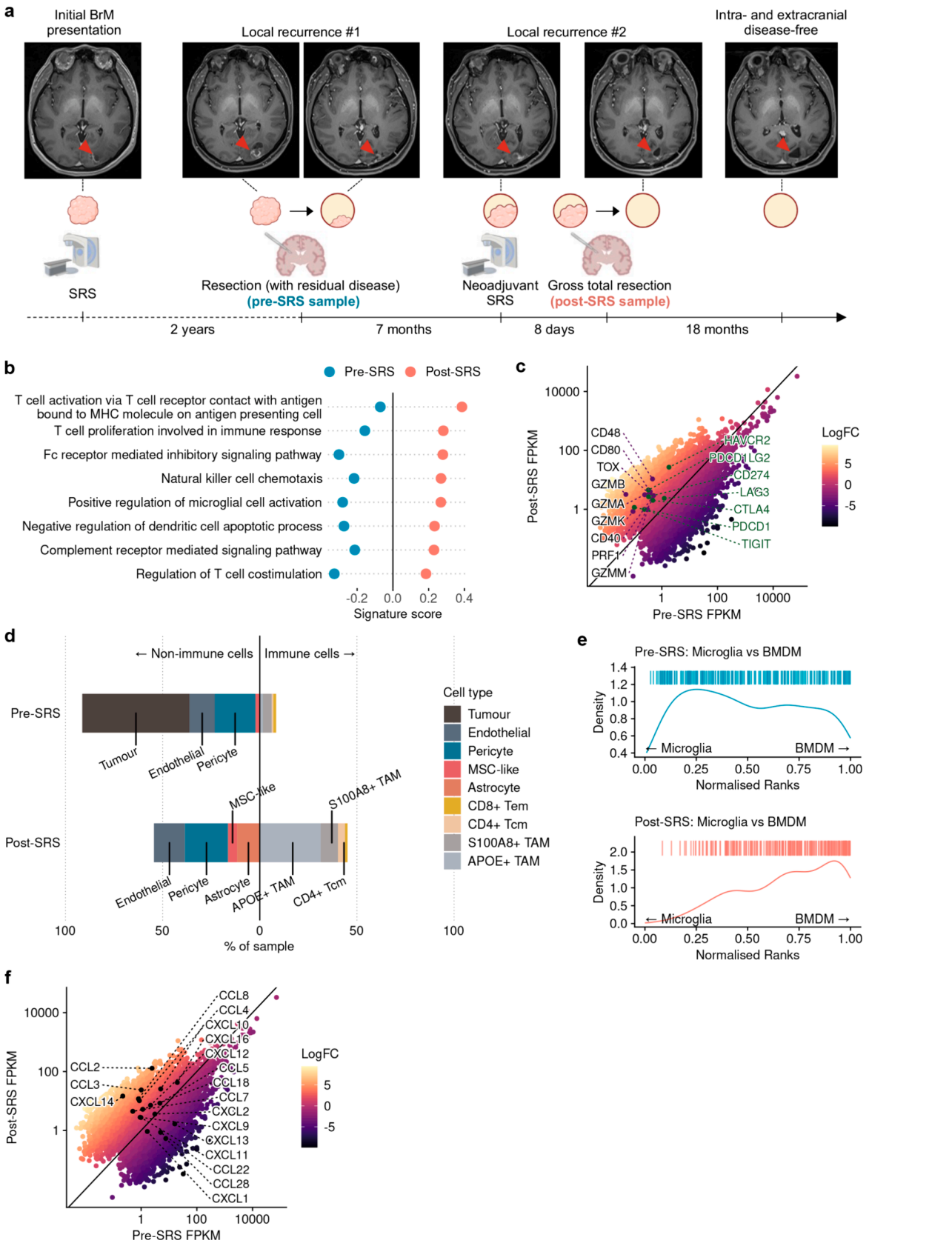

Fig. 2. Antigen presentation and T cell responses occur in the SRS-treated tumor A. Outline of patient case history, from whom longitudinal BrMs were obtained from the same location in the brain pre- and post-SRS. Arrowheads on magnetic resonance imaging (MRI) scans indicate the BrM of interest. **B.** Immune signatures among the top 30 Gene Ontology terms enriched following SRS. **C.** Gene expression correlation between pre- and post-SRS tumors. Selected key T cell genes are labelled. **D.** Cell type abundance from transcriptome deconvolution. **E.** Gene rank density plots of pre- and post-SRS tumors tested against a macrophage gene ontology signature. **F.** Gene expression correlation between pre- and post-SRS tumors. Cytokines are labelled.

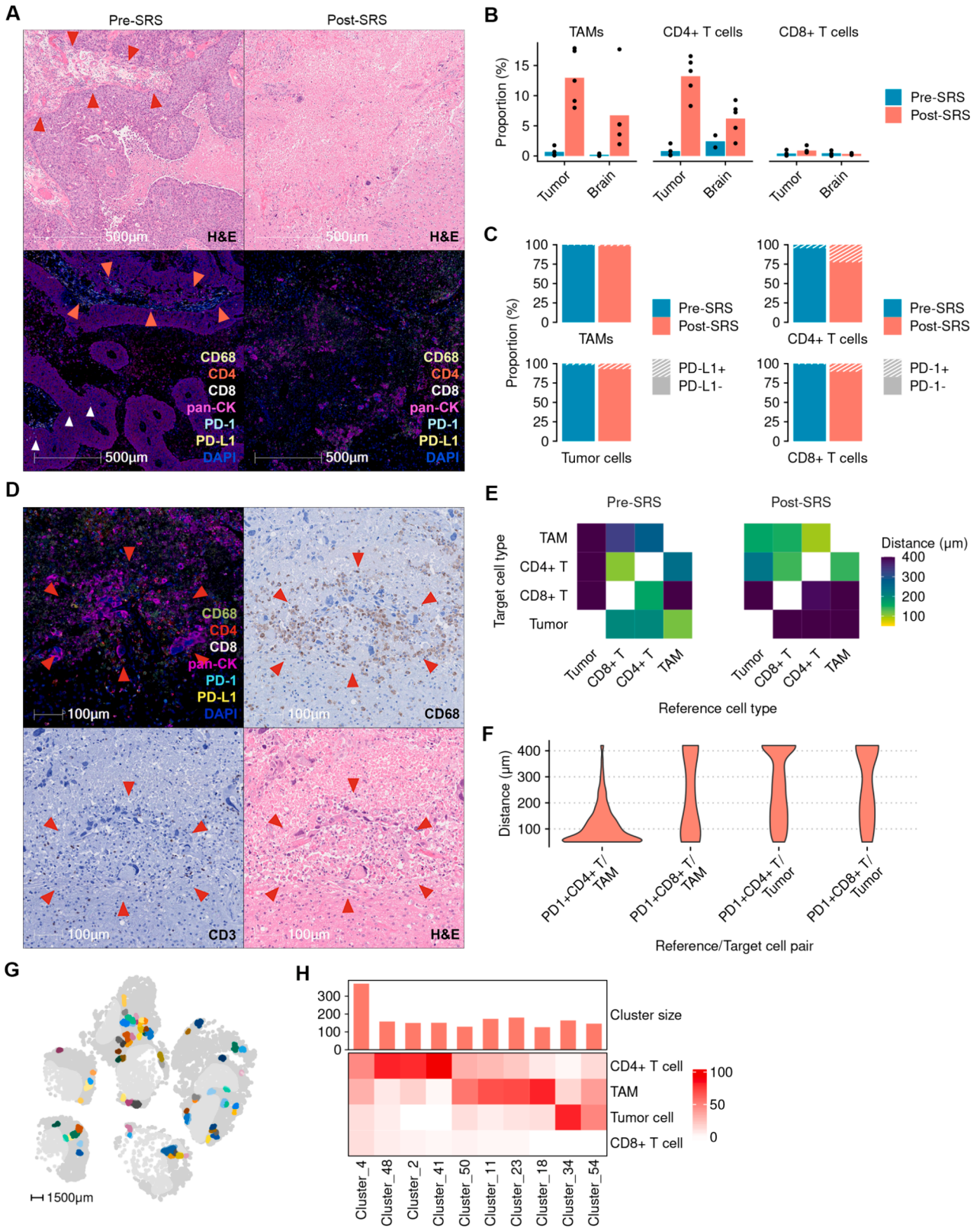

Fig. 3. Tumor-associated macrophages and CD4+ T cells cluster following SRS A Low magnification views of hematoxylin and eosin (H&E)-stained and multiplex immunohistochemistry (IHC) slides of pre- and post-SRS BrMs. Red arrowheads point to perivascular spaces outside tumor nests where immune cells segregated. White arrowheads point to sparse CD8+ T cells infiltrating tumor cell nests. **B.** Proportion of TAMs, CD4+ T cells, and CD8+ T cells in tumor and normal brain regions pre- and post-SRS by multiplex IHC. Each point represents cell count from a tissue fragment. **C.** Proportion of PD(L)-1+ TAMs, CD4+ T, CD8+ T and tumor cells pre- and post-SRS **D**. High magnification views of pre- and post-SRS BrMs. Arrowheads delineate a cluster of TAM, CD4+ T and tumor cells. **E.** Average minimum distances between cell types pre- and post-SRS. For all pairwise target/reference cell type comparisons pre- and post-SRS, adjusted p values were < 0.005. **F.** Violin plot of distances between PD1+ CD4+/CD8+ T cells and TAMs/tumor cells. **G.** Spatial plot of cell clusters in the post-SRS tumor. Bright grey areas represent normal brain parenchyma. **H.** Heatmap and bar plot of cell type abundance in the top 10 cell clusters.

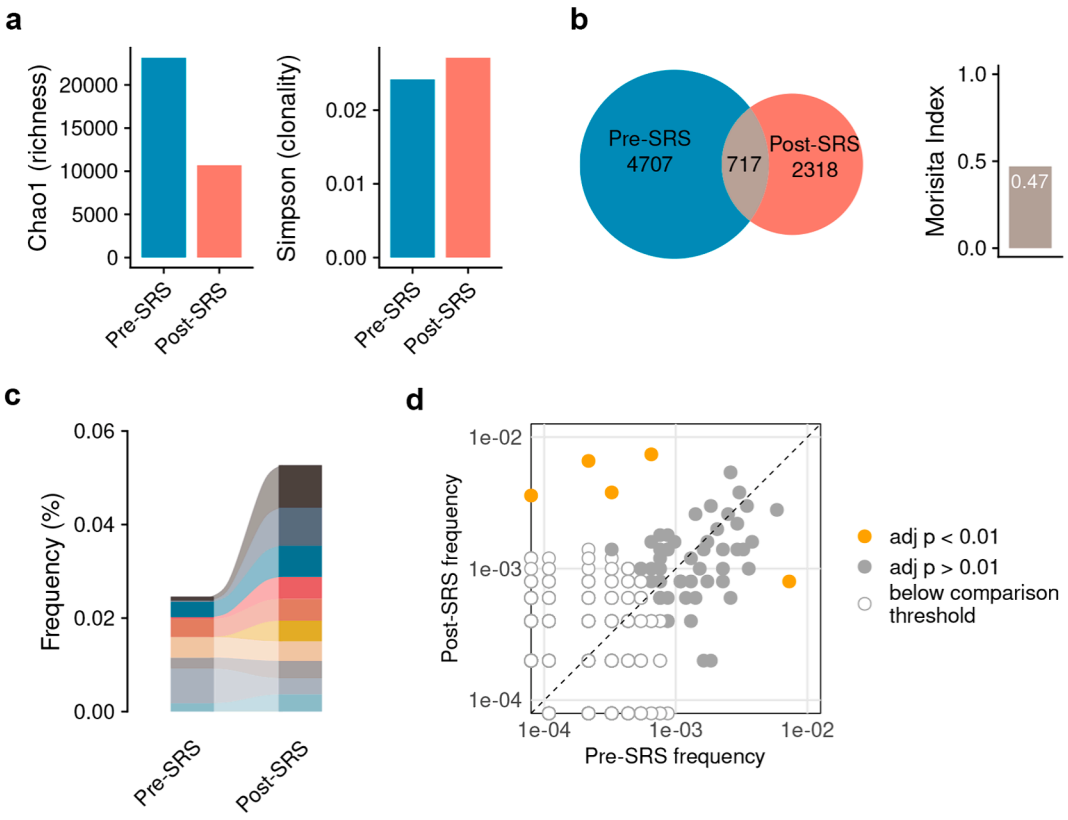

Fig. 4. T cell clones are retained and differentially abundant in the SRS-treated tumor A. TCR repertoire richness (Chao1 index) and clonality (Simpson index) in pre- and post-SRS tumors B Left: Distribution of TCR clones between pre- and post-SRS tumors. Right: TCR repertoire overlap between pre- and post-SRS tumors as calculated by the Morisita Index C. Pre-SRS tracking of the top 10 T cell clones in the post-SRS tumor. D. Differential abundance plot of TCR clones in the pre- and post-SRS tumors.

systemic and local immune responses by examining a unique set of patient-matched, longitudinal blood and tumour samples. We found SRS evoked an increase of classical and intermediate monocytes in the circulating bloodstream which likely trafficked into the SRS-treated tumour and differentiated in-situ into TAMs. CD4+ T cells were the second most enriched cell type in the post-SRS tumour. Interestingly, these were CD4+ T_{CM} cells by transcriptome deconvolution, which are the most abundant T cell subtype in the cerebrospinal fluid patrolling the central nervous system (CNS) [32]. The infiltration of macrophages into post-treatment brain tumours is not surprising, being professional phagocytes tasked with clearing of cellular debris. However, the strong antigen presentation and TCR engagement signatures, co-localisation of cells into TAM-CD4+ T cell-tumour cell clusters, and non-stochastic shifts in T cell clonal diversity suggest a possible SRS-induced adaptive immune response also occurring in the tumour milieu. The modulation of cDC, CD4+ and CD8+ T cells peripherally in our patient cohort may therefore be a related development, although this remains to be confirmed.

Strikingly, the importance of MHC-II-restricted TAM-CD4+ T cell interactions in preserving CD8+ T cell cytotoxicity and ICB response, but not CD8+ T cell abundance, in brain tumours was recently described [33]. While monocyte-derived macrophages are generally linked with immunosuppression and T cell exhaustion rather than T cell activation, macrophages adopt a spectrum of pro- and anti-tumour phenotypes that can be influenced by RT [34,35]. The majority of pre-SRS TAMs in our study were of the *S100A8+/FCN1+* subtype which more closely resembles MDSCs, whereas following SRS these were predominantly of the *APOE+/C1QB+*subtype which exhibits antigen processing and presentation programs [21]. In fact, a recent pre-clinical study showed that augmenting macrophages surprisingly generated CD8+ T cell-independent radiation abscopal responses [36].

Despite the focus on a single histology, our findings complement the larger state of knowledge beyond that for HER2-amplified breast cancers. The enrichment of peripheral T_{reg} cells following SRS for BrMs is consistent with similar observations following RT for extracranial tumours of various cancer types [37,38]. The increase in peripheral monocyte count was also described in a recent case report of SRS for 2 non-longitudinal NSCLC BrMs [13]. In that study, the predominant TAM subtype in the SRS-treated tumour was *FCN1+*, which in our study was only modestly elevated in comparison to *APOE+*TAMs. Furthermore, the authors found very low overlap in T cell repertoire between the SRS-treated and untreated BrMs (Morisita index of 0.01), concluding that SRS severely depleted tumour-resident T cells, almost fully replacing them with new clones from the circulating pool. In our study, the T cell repertoire overlap between pre- and post-SRS BrMs was substantially higher (Morisita index of 0.47). While we do not have matching data from circulating T cells to compare against, it is possible this amount of overlap may represent some retention of tumour-infiltrating T cells. These apparent discrepancies with our findings could be explained by the examination of two separate BrMs in that study, and that the irradiated BrM in that study was resected due to immediate disease progression, which introduce inter-tumour heterogeneity and primary treatment resistance as confounding factors.

Our study needs to be considered in light of its limitations. Firstly, only one pair of pre- and post-SRS BrMs was interrogated, which limits conclusions that can be made from this study. However, such samples are very rarely available for study, and despite this limitation, our findings challenge the limited data (or lack of) that underlie current assumptions. Secondly, we lack single-cell resolution data to confirm the biological contributions of each cell type and to ascribe T cell clones by CD4+ and CD8+ lineages. The targets of the differentially abundant TCRs are also unknown. Finally, because of limited tissue, we

intentionally designed our IHC panels with a macrophage and T cell focus, and thus were unable to discern other antigen presenting cell types such as cDCs that may have been present in the tumour.

Data availability

Raw sequencing data cannot be deposited in a public repository due to privacy concerns. Pre-processed RNA sequencing data are publicly available at https://doi.org/10.17632/6vc7hyd656.1.

Funding

Peter MacCallum Cancer Foundation Grant and Peter Mac Discovery Partner Fellowship to J.S. Cancer Council Victoria Colebatch Fellowship to S.S.

CRediT authorship contribution statement

Joseph Sia: Conceptualization, Methodology, Writing – original draft, Writing – review & editing, Funding acquisition. **Criselle D'Souza:** Methodology, Investigation, Writing – review & editing. **Becky Castle:** Investigation. **Yu-Kuan Huang:** Methodology, Writing – review & editing. **Han Xiang Aw Yeang:** Investigation, Writing – review & editing. **Rejhan Idrizi:** Investigation, Writing – review & editing. **Metta Jana:** Methodology, Writing – review & editing. **Shankar Siva:** Writing – review & editing, Resources. **Claire Phillips:** Writing – review & editing, Resources, Supervision. **Paul Neeson:** Writing – review & editing, Resources, Supervision.

Declaration of competing interest

The authors declare that they have no known competing financial interests or personal relationships that could have appeared to influence the work reported in this paper.

Acknowledgements

We thank Dr. Samuel Roberts-Thomson for assisting with delineating tumour and normal brain regions on the IHC slides. Icons in Fig. 1a and 2a were taken with permission from BioRender.

Appendix A. Supplementary data

Supplementary data to this article can be found online at https://doi.org/10.1016/j.ctro.2024.100863.

References

[1] Lamba N, Wen PY, Aizer AA. Epidemiology of brain metastases and leptomeningeal disease. Neuro Oncol 2021;23:1447–56.
[2] Nieder C, Spanne O, Mehta MP, Grosu AL, Geinitz H. Presentation, patterns of care, and survival in patients with brain metastases. Cancer 2011;117:2505–12.
[3] Tawbi HA, Forsyth PA, Hodi FS, Algazi AP, Hamid O, Lao CD, et al. Long-term outcomes of patients with active melanoma brain metastases treated with combination nivolumab plus ipilimumab (CheckMate 204): final results of an open-label, multicentre, phase 2 study. Lancet Oncol 2021;22:1692–704.
[4] Margolin K, Ernstoff MS, Hamid O, Lawrence D, McDermott D, Puzanov I, et al. Ipilimumab in patients with melanoma and brain metastases: an open-label, phase 2 trial. Lancet Oncol 2012;13:459–65.
[5] Goldberg SB, Schalper KA, Gettinger SN, Mahajan A, Herbst RS, Chiang AC, et al. Pembrolizumab for management of patients with NSCLC and brain metastases: long-term results and biomarker analysis from a non-randomised, open-label, phase 2 trial. Lancet Oncol 2020;21:655–63.
[6] Lehrer EJ, Peterson J, Brown PD, Sheehan JP, Quinones-Hinojosa A, Zaorsky NG, et al. Treatment of brain metastases with stereotactic radiosurgery and immune checkpoint inhibitors: An international meta-analysis of individual patient data. Radiother Oncol 2019;130:104–12.
[7] Kotecha R, Kim JM, Miller JA, Juloori A, Chao ST, Murphy ES, et al. The impact of sequencing PD-1/PD-L1 inhibitors and stereotactic radiosurgery for patients with brain metastasis. Neuro Oncol 2019;21:1060–8.
[8] Chen L, Douglass J, Kleinberg L, Ye X, Marciscano AE, Forde PM, et al. Concurrent immune checkpoint inhibitors and stereotactic radiosurgery for brain metastases in non-small cell lung cancer, melanoma, and renal cell carcinoma. Int J Radiat Oncol Biol Phys 2018;100:916–25.
[9] An Y, Jiang W, Kim BYS, Qian JM, Tang C, Fang P, et al. Stereotactic radiosurgery of early melanoma brain metastases after initiation of anti-CTLA-4 treatment is associated with improved intracranial control. Radiother Oncol 2017;125:80–8.
[10] Galluzzi L, Aryankalayil MJ, Coleman CN, Formenti SC. Emerging evidence for adapting radiotherapy to immunotherapy. Nat Rev Clin Oncol 2023;20:543–57.
[11] Simon Davis DA, Atmosukarto, II, Garrett J, Gosling K, Syed FM, Quah BJ. Irradiation immunity interactions. J Med Imaging Radiat Oncol. 2022.
[12] Churilla TM, Chowdhury IH, Handorf E, Collette L, Collette S, Dong Y, et al. Comparison of local control of brain metastases with stereotactic radiosurgery vs surgical resection: a secondary analysis of a randomized clinical trial. JAMA Oncol 2019;5:243–7.
[13] Hudson WH, Olson JJ, Sudmeier LJ. Immune microenvironment remodeling after radiation of a progressing brain metastasis. Cell Rep Med 2023;4:101054.
[14] Fischer GM, Jalali A, Kircher DA, Lee WC, McQuade JL, Haydu LE, et al. Molecular profiling reveals unique immune and metabolic features of melanoma brain metastases. Cancer Discov 2019;9:628–45.
[15] Chua KLM, Fehlings M, Yeo ELL, Nardin A, Sumatoh H, Chu PL, et al. High-dimensional characterization of the systemic immune landscape informs on synergism between radiation therapy and immune checkpoint blockade. Int J Radiat Oncol Biol Phys 2020;108:70–80.
[16] McGee HM, Daly ME, Azghadi S, Stewart SL, Oesterich L, Schlom J, et al. Stereotactic ablative radiation therapy induces systemic differences in peripheral blood immunophenotype dependent on irradiated site. Int J Radiat Oncol Biol Phys 2018;101:1259–70.
[17] Phillips C, Pinkham MB, Moore A, Sia J, Jeffree RL, Khasraw M, et al. Local hero: A phase II study of local therapy only (stereotactic radiosurgery and / or surgery) for treatment of up to five brain metastases from HER2+ breast cancer. (TROG study 16.02). Breast (Edinburgh, Scotland). 2024;74:103675.
[18] Wang M, Huang YK, Kong JC, Sun Y, Tantalo DG, Yeang HXA, et al. High-dimensional analyses reveal a distinct role of T-cell subsets in the immune microenvironment of gastric cancer. Clin Transl Immunology 2020;9:e1127.
[19] Hanzelmann S, Castelo R, Guinney J. GSVA: gene set variation analysis for microarray and RNA-seq data. BMC Bioinf 2013;14:7.
[20] Newman AM, Steen CB, Liu CL, Gentles AJ, Chaudhuri AA, Scherer F, et al. Determining cell type abundance and expression from bulk tissues with digital cytometry. Nat Biotechnol 2019;37:773–82.
[21] Gonzalez H, Mei W, Robles I, Hagerling C, Allen BM, Hauge Okholm TL, et al. Cellular architecture of human brain metastases. Cell 2022;185. 729-45.e20.
[22] Feng Y, Yang T, Zhu J, Li M, Doyle M, Ozcoban V, et al. Spatial analysis with SPIAT and spaSim to characterize and simulate tissue microenvironments. Nat Commun 2023;14:2697.
[23] Vadim I. Nazarov VOT, Siarhei Fiadziushchanka, Eugene Rumynskiy, Aleksandr A. Popov, Ivan Balashov, Maria Samokhina. immunarch: Bioinformatics Analysis of T-Cell and B-Cell Immune Repertoires. 2023.
[24] Shugay M, Bagaev DV, Zvyagin IV, Vroomans RM, Crawford JC, Dolton G, et al. VDJdb: a curated database of T-cell receptor sequences with known antigen specificity. Nucleic Acids Res 2018;46:D419–27.
[25] Tickotsky N, Sagiv T, Prilusky J, Shifrut E, Friedman N. McPAS-TCR: a manually curated catalogue of pathology-associated T cell receptor sequences. Bioinformatics 2017;33:2924–9.
[26] Collin M, Bigley V. Human dendritic cell subsets: an update. Immunology 2018; 154:3–20.
[27] Veglia F, Perego M, Gabrilovich D. Myeloid-derived suppressor cells coming of age. Nat Immunol 2018;19:108–19.
[28] Kurzrock R. Stem cell factor. In: Kufe D, Pollock R, Weichselbaum R, editors. Holland-Frei Cancer Medicine. 6th ed. Hamilton (ON): BC Decker; 2003.
[29] Sia J, Paul E, Dally M, Ruben J. Stereotactic radiosurgery for 318 brain metastases in a single Australian centre: the impact of histology and other factors. Journal of Clinical Neuroscience : Official Journal of the Neurosurgical Society of Australasia 2015;22:303–7.
[30] Scott AC, Dündar F, Zumbo P, Chandran SS, Klebanoff CA, Shakiba M, et al. TOX is a critical regulator of tumour-specific T cell differentiation. Nature 2019;571: 270–4.
[31] Müller S, Kohanbash G, Liu SJ, Alvarado B, Carrera D, Bhaduri A, et al. Single-cell profiling of human gliomas reveals macrophage ontogeny as a basis for regional differences in macrophage activation in the tumour microenvironment. Genome Biol 2017;18:234.
[32] Ellwardt E, Walsh JT, Kipnis J, Zipp F. Understanding the Role of T Cells in CNS Homeostasis. Trends Immunol 2016;37:154–65.
[33] Kilian M, Sheinin R, Tan CL, Friedrich M, Krämer C, Kaminitz A, et al. MHC class II-restricted antigen presentation is required to prevent dysfunction of cytotoxic T cells by blood-borne myeloids in brain tumours. Cancer Cell 2023;41. 235-51.e9.
[34] Ginhoux F, Schultze JL, Murray PJ, Ochando J, Biswas SK. New insights into the multidimensional concept of macrophage ontogeny, activation and function. Nat Immunol 2016;17:34–40.
[35] Becherini C, Lancia A, Detti B, Lucidi S, Scartoni D, Ingrosso G, et al. Modulation of tumour-associated macrophage activity with radiation therapy: a systematic review. Strahlentherapie Und Onkologie : Organ Der Deutschen Rontgengesellschaft [et Al] 2023;199:1173–90.

[36] Nishiga Y, Drainas AP, Baron M, Bhattacharya D, Barkal AA, Ahrari Y, et al. Radiotherapy in combination with CD47 blockade elicits a macrophage-mediated abscopal effect. Nature Cancer 2022;3:1351–66.
[37] Siva S, Bressel M, Mai T, Le H, Vinod S, de Silva H, et al. Single-fraction vs multifraction stereotactic ablative body radiotherapy for pulmonary oligometastases (SAFRON II): the trans tasman radiation oncology group 13.01 phase 2 randomized clinical trial. JAMA Oncol. 2021;7:1476-85.
[38] Formenti SC, Rudqvist NP, Golden E, Cooper B, Wennerberg E, Lhuillier C, et al. Radiotherapy induces responses of lung cancer to CTLA-4 blockade. Nat Med 2018; 24:1845–51.